Available online at www.sciencedirect.com
ScienceDirect
Journal of Molecular Catalysis A: Chemical 266 (2007) 158–165
JOURNAL OF MOLECULAR CATALYSIS A: CHEMICAL
www.elsevier.com/locate/molcata

Enhanced photocatalytic degradation of 4-chlorophenol by Zr^{4+} doped nano TiO_2

N. Venkatachalam, M. Palanichamy, Banumathi Arabindoo, V. Murugesan *

Department of Chemistry, Anna University, Chennai 25, India

Received 14 September 2006; accepted 24 October 2006
Available online 7 November 2006

Abstract

Zr^{4+} doped nano titania was prepared by sol–gel method using titanium(IV) isopropoxide and zirconium nitrate as precursors. The materials were characterized by XRD, BET, UV–vis, FT-IR, SEM-EDX and TEM techniques. The nanoparticles of pure TiO_2 contained both anatase and rutile phases together but Zr^{4+} doped TiO_2 gave anatase phase only. The framework substitution of Zr^{4+} in TiO_2 was established by XRD, SEM-EDX and FT-IR techniques. The band gap value of Zr^{4+} doped TiO_2 was higher than the parent nano TiO_2. TEM observations confirmed the nanocrystalline nature of Zr^{4+} doped TiO_2. The presence of dopants therefore could suppress the growth of TiO_2 grains, increase the surface area, decrease the anatase–rutile phase transformation and accelerate the surface hydroxylation. These properties resulted higher photocatalytic activity for Zr^{4+} doped nano TiO_2 than undoped nano TiO_2. The presence of anatase type structure in TiO_2 with high crystallinity and high phase stability, even after annealing at 800 °C substantially indicated that the dopants might inhibit densification and crystallite growth by providing dissimilar boundaries. The photocatalytic activity in the degradation of 4-chlorophenol was found to be higher for Zr^{4+} doped TiO_2 than both nano TiO_2 and commercial TiO_2 (Degussa P25). The experimental parameters such as initial concentration of 4-chlorophenol, catalyst loading, pH and light intensity were optimized for maximum degradation efficiency.

Keywords: Nano TiO_2; Metal doping; Anatase phase; 4-Chlorophenol; Mineralization

1. Introduction

4-Chlorophenol (4-CP), a known toxic and non-biodegradable organic compound, is present in the wastewater of pulp and paper, dyestuff, pharmaceutical and agrochemical industries. This compound is currently removed from the wastewater by conventional treatment methods such as biological treatment, chlorination and adsorption. However, the biological process usually requires considerably long treatment period to break down 4-CP, thus leading to unacceptable level in the final effluent [1]. Chlorination poses another problem since it often generates carcinogenic by-products. Granular activated carbon adsorption is the other commercialized process but the spent carbon needs to be disposed safely [2]. Semiconductor mediated photocatalytic oxidation has been accepted as a promising alternative to the conventional methods because most of the pollutants can be completely mineralized to CO_2 with suitable catalysts in the presence of UV light illumination. Among the semiconductors employed, TiO_2 is proved to be a good photocatalyst because of its high photosensitivity, non-toxicity, easy availability, strong oxidizing power and long-term stability [3–5].

Despite the positive attributes of TiO_2, the main drawback associated with its use is that most of the activated charge carriers will undergo recombination before reaching the surface to interact with adsorbed molecules. In fact, 90% of the generated carriers are lost within nanosecond of their generation, leading to low photoactivity of TiO_2. To circumvent the limitation, numbers of strategies have been proposed to improve the light absorption features and lengthen the carrier life time characteristics of the photocatalysts [6–8].

The influence of transition metal ions on the photoactivity of pure TiO_2 has been studied with the aim to improve the efficiency of the photocatalytic process. It has been hypothesized that the incorporation of transition metal ions on titania increases the rate of photocatalytic oxidation due to the electron scaveng-

* Corresponding author. Tel.: +91 44 22203144; fax: +91 44 22200660/22350397.
E-mail address: v_murugu@hotmail.com (V. Murugesan).

1381-1169/$ – see front matter © 2006 Elsevier B.V. All rights reserved.
doi:10.1016/j.molcata.2006.10.051

ing effect of the metal ions on the surface of TiO_2. Most of the metal doped TiO_2 were prepared by co-precipitation or incipient wet impregnation method [9]. Substitution of metal ions in the bulk TiO_2 crystallites is not likely to occur in the impregnation method and at the best substitution may take place on the surface of TiO_2. In the co-precipitation method, post heat processing of mixed metal hydroxides yields metal doped TiO_2. This high temperature and long time heating may separate out the dopant metal ion into respective metal oxide and in many cases it segregates on the surface of TiO_2 [10].

Mechanochemical doping, hydrothermal crystallization and metal organic vapor deposition are the other methods that have been reported for the preparation of metal doped TiO_2. Comparison of the results reported in the literature for doped TiO_2 samples is difficult since the preparation methods of the photocatalysts are usually different [11,12]. It has been shown that the photocatalytic activity of TiO_2 can be influenced by its crystal structure, surface area, size distribution, porosity, band gap and surface hydroxyl group density. Most of the studies have been focused on the preparation of nanosized TiO_2 with a view to improve the light absorption capacity. Additionally, the small size of TiO_2 particles can make indirect band electron transition and thus increase the generation rate of electrons and holes.

Recently, sol–gel method is proved to be a novel technique for the preparation of nanocrystalline TiO_2. It has been demonstrated that the physiochemical and electrochemical properties of TiO_2 can be modified to improve its efficiency by sol–gel method. Since this method is a solution process, it has all the advantages of wet chemical process such as control of stoichiometry, doping of desired amount of transition metal ions, and fine dispersion of the dopant and titanium source. Generally, particle size is an important parameter for photocatalysis since it directly impacts the specific surface area of a catalyst. With a small particle size, the number of active surface sites increases and so does the surface charge carrier transfer rate in photocatalysis [13–16]. The physiochemical properties of Zr^{4+} doped nano TiO_2 and correlation of these properties in the photocatalytic activity of TiO_2 for 4-chlorophenol (4-CP) degradation are presented in this manuscript.

2. Experimental

2.1. Materials and methods

All the chemicals were obtained from Merck (India) and used as such without further purification. The commercially available TiO_2 (Degussa P25) was obtained from Degussa Chemical, Germany. The typical synthesis procedure for nano TiO_2 and metal doped nano TiO_2 is as follows: titanium(IV) isopropoxide, glacial acetic acid and water were maintained in a molar ratio 1:10:350. Titanium(IV) isopropoxide (18.6 ml) was hydrolyzed using 35.8 ml glacial acetic acid at 0 °C. To this solution 395 ml water was added drop wise under vigorous stirring for 1 h and continued the stirring for further 5 h until a clear solution of TiO_2 nanocrystals was formed. The prepared solution was kept in the dark for nucleation process for 24 h. After the period, the solution was placed in an oven at a temperature of 70 °C for a period of 12 h for the gelation process. The gel was then dried at 100 °C and subsequently the catalyst was crushed into fine powder and calcined in a muffle furnace at 500 °C for 5 h. In the preparation of Zr^{4+} doped TiO_2, requisite amount of zirconium nitrate (0.3, 0.5, 0.7, 1.0, 2.0 and 3.0 mol%) was dissolved in 395 ml water and the above procedure was adopted as such.

2.2. Catalyst characterization and analytical method

The XRD patterns were recorded on a PANAalytical X′ pert PRO X-ray diffractometer using Cu Kα radiation as the X-ray source. The diffractograms were recorded in the 2θ range 10–80° in steps of 0.02° with a count time of 20 s at each point. The average crystallite size of anatase and rutile phases was determined according to the Scherrer equation using the full width at half maximum (FWHM) data of each phase after correcting the instrumental broadening. The specific surface area (BET method), specific pore volume and average pore diameter (BJH method) of the samples were determined by nitrogen adsorption–desorption isotherms using Quantochrome Autosorb 1 sorption analyzer. The calcined samples were outgassed at 250 °C under vacuum (10^{-5} mbar) for 3 h prior to adsorption experiments. The particle size and morphology of nano TiO_2 and Zr^{4+} doped TiO_2 were observed using transmission electron microscope (TEM) (JEOL 3010) and scanning electron microscope (SEM) (Stereo scan LEO 440). The emission spectra of the catalyst samples were recorded using spectrofluorometer (Horiba Fluromax-2) at the excitation wavelength of 290 nm. UV–vis absorption spectra of the catalyst samples were recorded using UV–vis spectrophotometer (Shimadzu 2601). FT-IR spectra of the samples were recorded on a FI-IR spectrometer (Nicolet Avatar 360). The extent of 4-CP degradation was monitored using UV–vis spectrophotometer (Shimadzu1601) and high performance liquid chromatograph (HPLC) (Shimadzu LC10 ATVP series equipped with UV–vis detector). The intermediates were identified using gas chromatograph coupled with mass spectrometer (GC–MS) (Perkin-Elmer Clarus 500). The extent of mineralization was determined using a total organic carbon analyzer (TOC) (Shimadzu V_{CPN}).

2.3. Adsorption study

Prior to photocatalytic experiments, adsorption of 4-CP on the catalyst surface was carried out by mixing 100 ml of aqueous solution of 4-CP (250 mg/l) with a fixed weight of the catalyst (200 mg) at pH 5. Aliquots were withdrawn at specific time intervals and the change in 4-CP concentration was measured by HPLC. The extent of equilibrium adsorption was determined from the decrease in 4-CP concentration. From the adsorption experiments, the percentage of 4-CP adsorbed on the catalyst surface was determined from the following equation:

$$\%\ \text{of 4-CP adsorbed} = \frac{C_0 - C_t}{C_0} \times 100$$

where C_0 is the initial concentration of 4-CP and C_t is the concentration of 4-CP after t minutes.

2.4. Photocatalytic studies

The cylindrical photochemical reactor was made up of quartz glass with a dimension of 30 cm × 3 cm (height × diameter). The top portion of the reactor has ports for sampling, gas purging and gas outlet. The aqueous 4-CP solution containing appropriate quantity of either nano TiO_2 or Zr^{4+} doped TiO_2 was taken in the quartz reactor and subjected to aeration for thorough mixing. The set-up was placed inside the reactor which was 6.5 cm away from the lamps. The lamp housing consisted of low-pressure mercury lamps (8 × 8 W) emitting 365 nm with polished anodized aluminium reflectors and black cover to prevent UV leakage. The photocatalytic degradation was carried out with 100 ml aqueous 4-CP solution (250 mg/l) and 200 mg nano TiO_2 or Zr^{4+} doped TiO_2 photocatalyst. The experiments were performed at room temperature and the pH of reaction mixture was kept at 5. Prior to irradiation, the slurry was aerated for 30 min to reach adsorption equilibrium followed by UV irradiation. Adequate aliquots of the sample were withdrawn after periodic interval of irradiation and analyzed after centrifugation. Since optimization of reaction variables will maximize the degradation efficiency, reaction parameters like initial 4-CP concentration, catalyst loading and solution pH were optimized.

3. Results and discussion

3.1. Physiochemical characterization

The XRD patterns of nano TiO_2 and Zr^{4+} doped nano TiO_2 are shown in Fig. 1. Though the patterns of nano TiO_2 calcined at 500 °C correspond to both anatase and rutile forms (Fig. 1a), anatase phase is the predominating one. The XRD patterns of 1 mol% Zr^{4+} doped TiO_2 indicate complete absence of rutile phase (Fig. 1b). The doped TiO_2 samples devoid of amorphous structures. It can be seen that increase of calcination temperature from 400 to 600 °C, the peak intensity of anatase increases and the width of (1 0 1) plane at $2\theta = 25.3^\circ$ becomes narrow. The

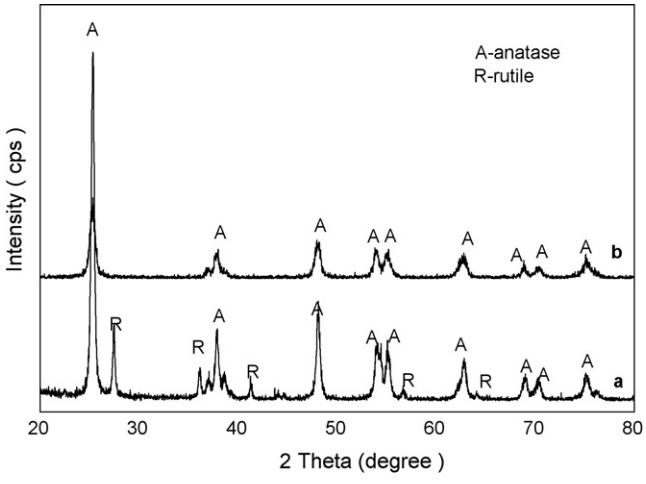

Fig. 1. XRD patterns of TiO_2 calcined at 500 °C (a) nano TiO_2 and (b) 1 mol% Zr^{4+} doped TiO_2.

rutile phase starts appearing at 500 °C for pure nano TiO_2 but the rutile peaks appear only at 700 °C for Zr^{4+} doped TiO_2. Thus, the dopant is expected to play a significant control on the selective crystallization of anatase phase during the sol–gel process [17,18]. The close examination of XRD patterns of both nano TiO_2 and Zr^{4+} doped TiO_2 illustrates the existence of splitting of peaks at 62.79°, 68.77°, 70.33° and 75.09° (2θ). The average particle size was estimated by applying the Scherrer formula on the anatase (1 0 1) and rutile (1 1 0) diffraction peaks (the most intense peak for each phase):

$$D = \frac{K\lambda}{\beta \cos\theta}$$

where D is the crystal size of the catalyst, λ the X-ray wavelength (1.54 Å), β the full width at half maximum (FWHM) of the catalyst, $K = 0.89$ and θ is the diffraction angle. An average crystal size from 6 to 12 nm (Table 1) was obtained for Zr^{4+} doped TiO_2 samples. As a result of calcination, there is enhanced intensity for all the patterns compared to uncalcined TiO_2. Hence, there might be condensation of free defective OH groups to form TiO_2 with high percentage crystallinity. The diffraction patterns of Zr^{4+} doped TiO_2 (up to 5 mol%) calcined at 500 °C show typical peaks of TiO_2 nanocrystalline anatase phase without any detectable dopant related peaks. Hence, the dopant may be occupied either interstitial positions or substitutional sites of the TiO_2 crystal structure. The nanocrystalline anatase structure for Zr^{4+} doped TiO_2 was confirmed by (1 0 1), (0 0 4), (2 0 0), (1 0 5) and (2 1 1) diffraction peaks. Since Zr^{4+} is more electropositive than Ti^{4+}, the electronic cloud in each TiO_2 nanoparticle might be loosely held, thus favoring formation of less dense anatase phase. In other words, the tight packing arrangements required for rutile phase formation is fully suppressed by the addition of zirconium nitrate in water which enhances the polarity of water, thus facilitating the formation of anatase phase only. The entry of Zr^{4+} in the lattice of TiO_2 prevents interconversion of anatase to rutile during calcination. Since Zr^{4+} is larger in size and more electropositive character than Ti^{4+}, the lattice can exhibit better bonding property and thus higher thermal stability than pure TiO_2. However, 5 mol% Zr^{4+} doped TiO_2 (Fig. 2) did not give any peak corresponding to ZrO_2 and better existence of peak splitting in anatase phase. Hence, it might be amorphous or below the detectability limit of XRD but the intensity of anatase peaks decreased and the splitting of anatase peaks were well resolved. This is due to the formation of nanosize particles in the range undetectable by XRD in addition to those that are detectable. The formation of TiO_2 particles of size less than even 4 nm is also evident from TEM analysis.

Table 1 presents the textural properties of nano TiO_2 and Zr^{4+} doped TiO_2. It can be seen that the specific surface area shifts towards lower values at higher calcination temperatures. The surface area of the catalysts increased with increase of Zr^{4+} content. This increase may be due to Zr^{4+} present on the surface of TiO_2 which inhibits densification and crystalline growth of TiO_2 nanoparticles by providing dissimilar boundaries. Fig. 3 illustrates the pore size distribution curve calculated from the desorption branch of nitrogen adsorption isotherm by BJH

Table 1
Textural and structural properties of nano TiO_2 and Zr^{4+} doped nano TiO_2

Catalyst	Specific surface area[a] (m^2/g)	Pore diameter[b] (nm)	Particle size[c] (nm)	Band gap energy[d] (eV)	4-CP adsorbed (%)
Nano TiO_2	66	3.6	18–20	3.21	14.2
0.5 mol% Zr^{4+}-TiO_2	80	4.3	12–15	3.23	18.3
1.0 mol% Zr^{4+}-TiO_2	95	4.8	8–12	3.27	26.8
2.0 mol% Zr^{4+}-TiO_2	125	5.2	6–12	3.29	29.6
3.0 mol% Zr^{4+}-TiO_2	133	5.6	4–10	3.31	34.2
5.0 mol% Zr^{4+}-TiO_2	139	5.1	4–12	3.31	37.4

[a] BET surface area calculated from the linear portion of the BET plot in the relative pressure range of $p/p_0 = 0.05$–0.35.
[b] Average pore diameter estimated using adsorption branch of the isotherm.
[c] Particle size obtained from TEM pictures.
[d] Bandgap energy (eV) calculated using the formula BG = 1240/λ.

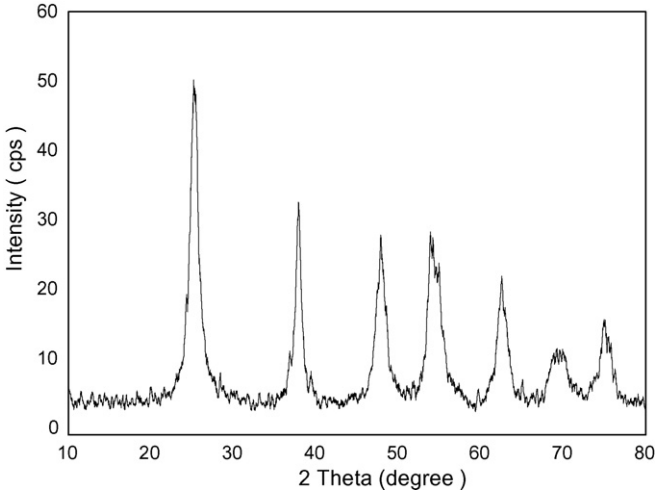

Fig. 2. XRD patterns of 5 mol% Zr^{4+} doped TiO_2 calcined at 500 °C.

method and the corresponding nitrogen adsorption–desorption isotherm of 3 mol% Zr^{4+} doped TiO_2 powder calcined at 500 °C for 5 h. The sharp decline in the desorption curve is indicative of mesoporosity while the hysteresis (type IV) between the two curves demonstrates that there is a diffusion bottle neck possibly caused by the non-uniform pore size of TiO_2 [19]. The pore size distribution graph reveals pore size range of 3–8 nm with an average pore diameter of 9.5 nm. These pores can allow rapid diffusion of 4-CP molecules during photocatalytic reaction. Zr^{4+} doped TiO_2 (3 mol%) calcined at 500 °C exhibits higher specific surface area (133 m^2/g), than that of TiO_2 (50 m^2/g) (Degussa P25).

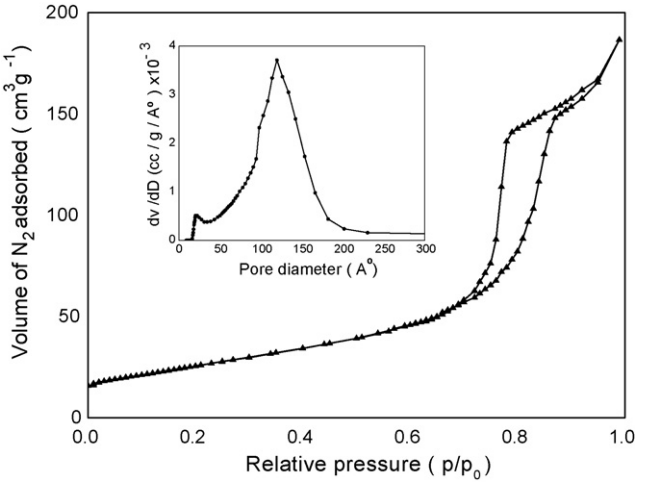

Fig. 3. Nitrogen adsorption–desorption isotherms and the corresponding pore size distribution curve calculated from desorption branch of the nitrogen isotherm (inset) of 3 mol% Zr^{4+} doped TiO_2 calcined at 500 °C.

SEM micrograph of calcined (500 °C) 1 mol% Zr^{4+} doped TiO_2 is shown in Fig. 4. It is observed that the doped nano TiO_2 particles are spherical with an average grain size of 10–12 nm, which is consistent with the XRD results. The EDX data of pure and Zr^{4+} doped TiO_2 are shown in Figs. 5 and 6. Nano TiO_2 shows a peak around 0.2 kev and another intense peak appears at 4.5 kev. The intense peak is assigned to TiO_2 in the bulk form and the less intense peak is assigned to surface TiO_2. The EDX patterns of Zr^{4+} doped TiO_2 are shown in Fig. 6. The peaks due to TiO_2 appear at the same position as shown in Fig. 5. The peaks due to Zr^{4+} are not clearly distinct in 1 mol% Zr^{4+} doped TiO_2 whereas one of the Zr^{4+} peaks appears intense in the case of 3 mol% Zr^{4+} doped TiO_2 which may be assigned to bulk Zr^{4+}. The less intense peak of Zr^{4+} is assigned to Zr^{4+} in the TiO_2 lattices. Figs. 7 and 8 are the TEM pictures and the corresponding histogram (particle size distribution) of 1 mol% Zr^{4+} doped TiO_2, both are proven the nanocrystalline nature of doped TiO_2.

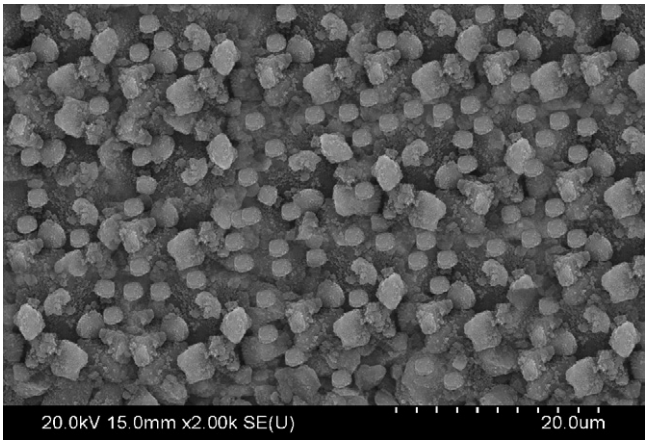

Fig. 4. SEM picture of 3 mol% Zr^{4+} doped TiO_2 calcined at 500 °C.

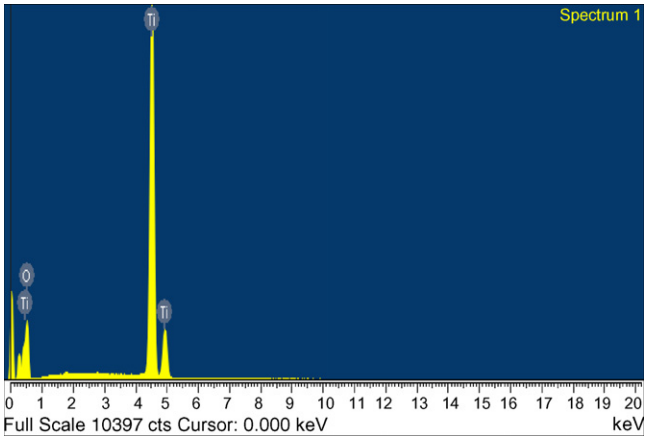

Fig. 5. EDX patterns of pure nano TiO_2 calcined at 500 °C.

FT-IR spectra of nano and Zr^{4+} doped TiO_2 show peaks corresponding to the stretching vibrations of O–H and bending vibrations of adsorbed water molecules around 3350–3450 and 1620–1635 cm^{-1}, respectively. The low intensity of these peaks with increase in the calcinations temperature is indicating the removal of large portion of adsorbed water from TiO_2 (not shown in figure). Fig. 9 shows a broad intense band below 1200 cm^{-1} which is due to Ti–O–Ti vibration. In addition, the surface hydroxyl groups in TiO_2 increase with increase of Zr^{4+} loading, which is not only favor the trapping of electrons to enhance the separation efficiency of electron–hole pair but also form surface free radical (•OH) to enhance the photocatalytic degradation of 4-CP [20].

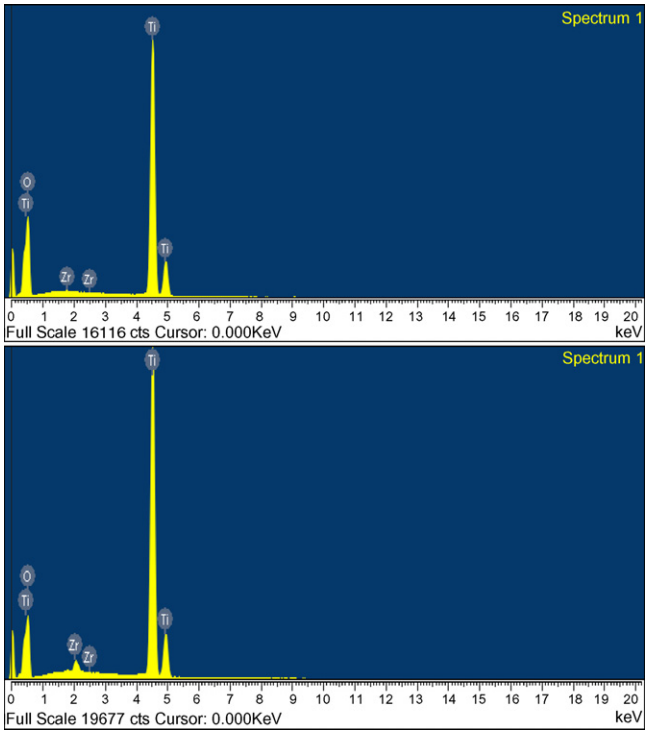

Fig. 6. EDX patterns of Zr^{4+} doped TiO_2 calcined at 500 °C: (a) 1 mol% Zr^{4+} doped TiO_2 and (b) 3 mol% Zr^{4+} doped TiO_2.

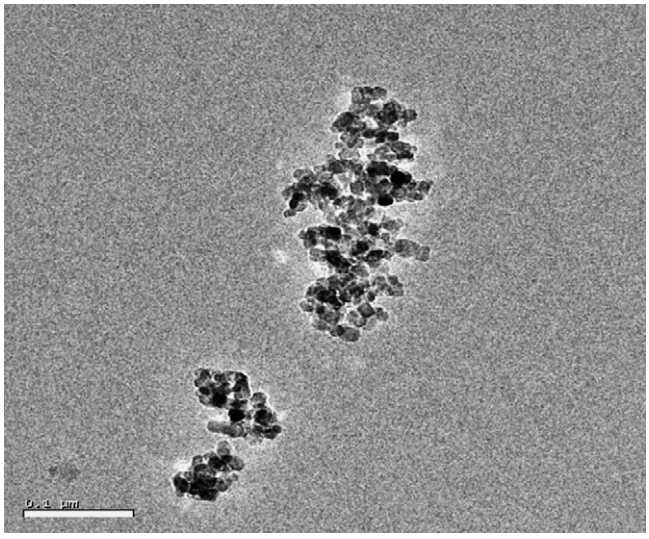

Fig. 7. TEM picture of 3 mol% Zr^{4+} doped TiO_2 calcined at 500 °C.

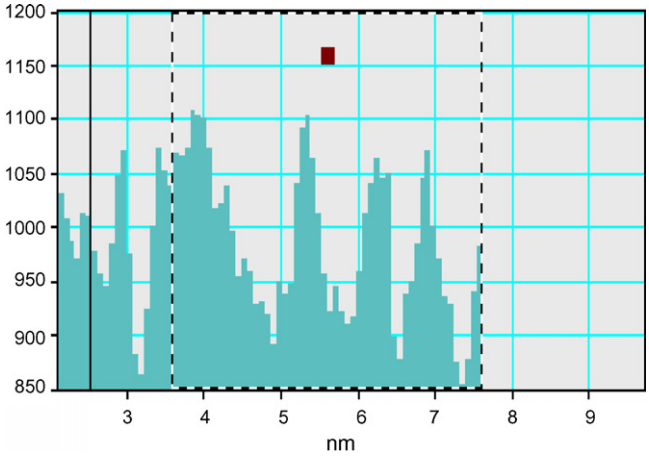

Fig. 8. Particle size distribution histogram of 3 mol% Zr^{4+} doped TiO_2 calcined at 500 °C.

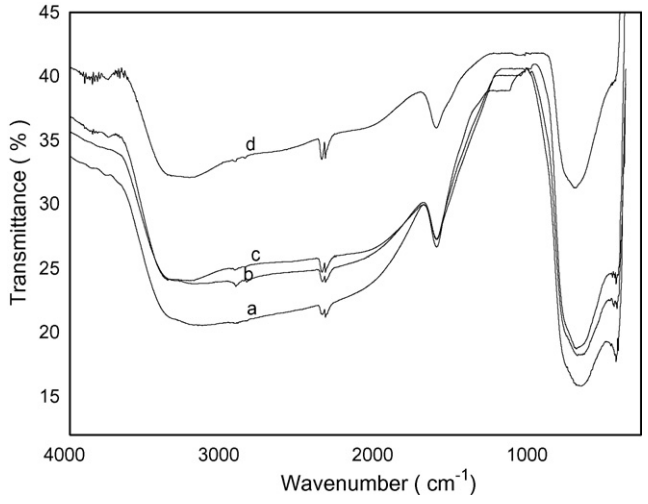

Fig. 9. FT-IR spectra of nano TiO_2 and Zr^{4+} doped TiO_2 calcined at 500 °C: (a) nano TiO_2, (b) 0.5 mol% Zr^{4+} doped TiO_2, (c) 1 mol% Zr^{4+} doped TiO_2 and (d) 3 mol% Zr^{4+} doped TiO_2.

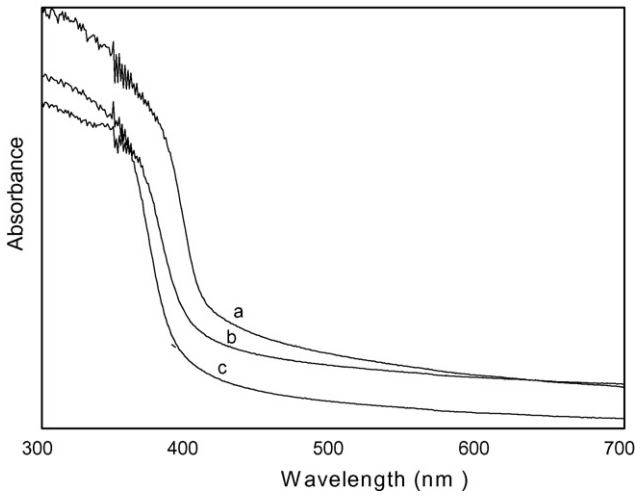

Fig. 10. UV–vis absorption spectra of nano TiO_2 and Zr^{4+} doped TiO_2 calcined at 500 °C: (a) nano TiO_2, (b) 1 mol% Zr^{4+} doped TiO_2 and (c) 3 mol% Zr^{4+} doped TiO_2.

UV–vis absorption spectra of nano and Zr^{4+} doped TiO_2 are shown in Fig. 10. The absorption spectrum of nano TiO_2 consists of a single and broad intense absorption around 400 nm due to charge-transfer from the valence band (mainly formed by 2p orbitals of the oxide anions) to the conduction band (mainly formed by 3d t_{2g} orbitals of the Ti^{4+} cations) [21]. Pure nano TiO_2 shows its absorption in the longer wavelength region than Zr^{4+} doped TiO_2. Hence, there is sufficient decrease in the particle size and increase in the band gap value due to Zr^{4+} doping. Furthermore, zirconium is in the +4 oxidation state and the valence band of TiO_2 consists of only the O (2p) band. This O (2p) band is stabilized more on Zr^{4+} doping since it is more electropositive than Ti^{4+}. Hence, there is an increase in the band gap of TiO_2 [22].

3.2. Optimization of reaction variables in the degradation of 4-CP

3.2.1. Effect of initial 4-CP concentration

The influence of initial 4-CP concentration on degradation rate was studied from 50 to 300 mg/l at a constant TiO_2 loading of 200 mg and a solution pH of 5. The volume of 4-CP solution was 100 ml. It was observed that the degradation rate increased with increase in concentration of 4-CP up to 250 mg/l and then decreased. The degradation followed pseudo-first-order kinetics at low 4-CP concentration, which is in accordance with our earlier reports [23]. The UV λ_{max} value of 4-CP is 280 nm. Hence, the absorption of UV light by the pollutant dominated at higher concentrations. The screening effect dominated at concentrations higher than 250 mg/l and hence degradation efficiency decreased. We have observed such type of screening effect in the degradation of dyes and pesticides in our earlier reports [23]. Furthermore, the formation of $^{\bullet}OH$ radicals is constant for a given amount of the catalyst and hence the available $^{\bullet}OH$ radicals are insufficient for 4-CP degradation at higher concentration [23].

3.2.2. Effect of catalyst dosage

A series of experiments were carried out to optimize the catalyst loading by varying the amount of nano TiO_2 from 100 to 500 mg in 100 ml 4-CP solution of concentration 250 mg/l. The rate of degradation increased linearly with increase in catalyst loading up to 200 mg and then decreased due to increase in turbidity of the solution, which interfere light transmission into the solution. The low degradation rate at higher catalyst loading may also due to deactivation of activated molecules by collision with ground state molecules of titania [24].

3.2.3. Effect of solution pH

Solution pH is an important variable in the evaluation of aqueous phase mediated photocatalytic degradation reactions. It influences adsorption and dissociation of the substrate, catalyst surface charge, oxidation potential of the valence band and other physiochemical properties. The role of pH on the rate of photocatalytic degradation was attempted under optimum concentration of 4-CP (250 mg/l) and TiO_2 (200 mg) by varying the initial pH values from 4 to 9. It is reported that the zero point charge (pH_{zpc}) of TiO_2 is 6.9 [5]. The rate of degradation in the acidic pH range (at 5) was found to be higher than the alkaline pH. The high degradation rate in the acidic pH is due to enhanced adsorption of 4-CP on the surface of TiO_2 that carries positive charge. In addition, minimization of electron–hole recombination in the acidic pH is also an additional important factor for the enhanced degradation of 4-CP. In the alkaline pH (at 9) both 4-CP and surface of TiO_2 carry negative charge and hence the degradation rate was found to be less [25].

3.2.4. Effect of light intensity

The effect of light intensity was investigated from 16 to 64 W. The results revealed that the degradation rate increased with increase in the light intensity up to 64 W. Electron–hole recombination is a commonly encountered problem in photocatalysis. In addition, excitation of every catalyst particle by light irradiation at any instant cannot be possible. But the probability of excitation can be increased by increasing the intensity of incident light. It also increases the reexcitation of recombined electrons. Hence, increase in the degradation rate was observed with increase in the intensity of incident light. The mineralization of 4-CP was studied with lamps of wavelength 365 and 254 nm over TiO_2 and compared their efficiency. Though the mineralization rates apparently appeared to be nearly equal for both the lamps, the mineralization rate at 365 nm is slightly higher than at 254 nm. Since the band gap excitation of electrons in TiO_2 with 254 nm can promote electrons to the conduction band with high kinetic energy, they can reach the solid–liquid interface easily, suppressing electron–hole recombination in comparison to 365 nm. The observation of low rate for 254 nm is therefore unexpected. This can be accounted by considering partial absorption and wasting of the light of 254 nm by 4-CP itself. Generally, the pollutants should possess negligible absorption close to the wavelength of irradiation source. Hence, the entire light of irradiation at 254 nm in the reactor is not used for the excitation of TiO_2 particles because of the intervening 4-CP molecules as well as those adsorbed on TiO_2 particles. Hence, absorption and wasting of

light at 254 nm by 4-CP might be the actual cause for less rate of degradation than at 365 nm.

3.3. Mineralization studies

The extent of degradation and mineralization of 4-CP was followed by UV–vis spectroscopy, HPLC and TOC analyzer. Compounds like hydroquinone and hydroxyhydroquinone were the predominant intermediates identified by GC–MS during the photocatalytic degradation of 4-CP, in which hydroquinone existed for longer period during the photocatalytic degradation of 4-CP. This may be due to the fact that hydroquinone in acidic medium can exist in equilibrium with quinone as shown in the following equation:

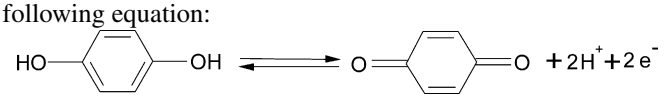

Thus, the released electron can neutralize the holes of TiO_2. The electron in the conduction band can also be easily trapped by quinone to form hydroquinone. Hence, the mineralization of hydroquinone by photocatalytic degradation is rather difficult. The decreasing trend in TOC against irradiation time in the degradation of 4-CP using Zr^{4+} doped TiO_2, nano TiO_2 and TiO_2 (Degussa P25) are depicted in Fig. 11. The TOC removal efficiency of TiO_2 (Degussa P25) and nano TiO_2 is lower than that of Zr^{4+} doped TiO_2. Under identical experimental conditions, mineralization of 4-CP required 300 min with 3 mol% Zr^{4+} doped TiO_2, 420 min with nano TiO_2 and 480 min with TiO_2 (Degussa P25).

The experimental results revealed that dopant in TiO_2 play significant role in the enhancement of photocatalytic activity. The experimental results also confirmed that the optimum doping molar ratio of Zr^{4+} ion and TiO_2 is found to be 3:97 and above this ratio, the structural and textural parameters of TiO_2 are affected. The entry of Zr^{4+} into the lattice of TiO_2 creates charge compensating anion vacancy in the lattice points of TiO_2 which may enhance the adsorption of 4-CP. In addition, the expected enhanced Lewis acidity of the catalyst is also an

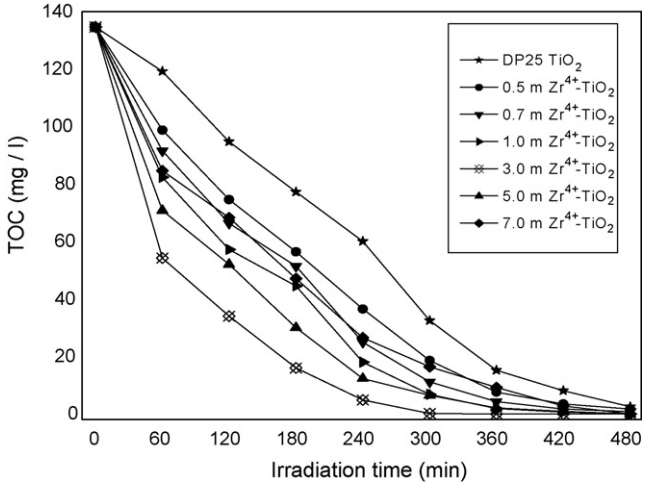

Fig. 11. Comparison of photocatalytic mineralization of nano TiO_2 and Zr^{4+} doped TiO_2 (experimental conditions: initial concentration of 4-CP = 250 mg/l, volume of 4-CP = 100 ml, solution pH 5 and catalyst dosage = 200 mg).

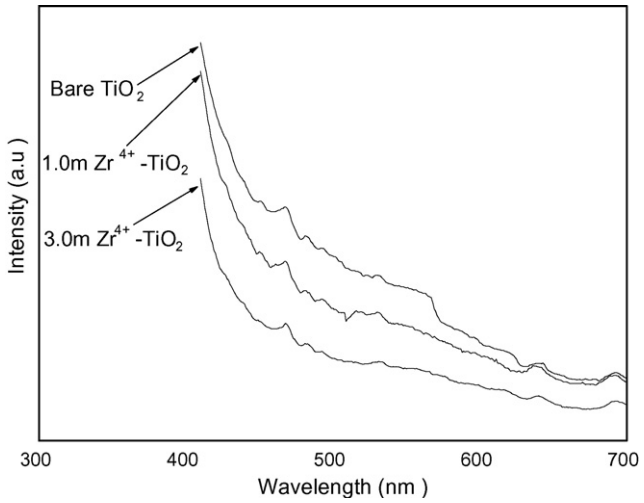

Fig. 12. Fluorescent emission spectra of nano TiO_2 and Zr^{4+} doped TiO_2 calcined at 500 °C.

important contributing factor for Zr^{4+} doped TiO_2. The Lewis acid sites act as electron traps and also act as effective adsorption sites to enhance the rate of photocatalytic degradation of 4-CP [26]. SEM observations also gave convincing evidence for the presence of zirconium on the surface of TiO_2. Further, the dopant ion Zr^{4+} with ionic radius (0.79 Å) closer to Ti^{4+} (0.75 Å) can either isomorphously substituted or interstitially introduced into the matrix of TiO_2 to produce oxygen vacancies which accelerate the transition and nanocrystallite growth of anatase TiO_2. The fluorescent emission spectra of Zr^{4+} doped TiO_2 (Fig. 12) also give convincing evidence for the oxygen vacancy in TiO_2. Since the excitation was carried out under equal adsorption conditions at 290 nm, decrease in emission intensity was observed with Zr^{4+} doped TiO_2 samples compared to pure nano TiO_2. The decrease in emission intensity may also due to the introduction of new defect sites such as oxide ion vacancy. The oxide ion vacancy can trap an electron in the following pathway. The ionized oxygen vacancy level is poised to trap rapidly the photogenerated conduction band electron which subsequently interacts with a valence band hole either radiatively or non-radiatively:

$$V_o^0 + e_{CB}^- \rightarrow V_0 \text{ (electron trapping in shallow traps)}$$

$$V_0 + h_{VB}^+ \rightarrow V_o^0 + h\nu \text{ (radiative recombination)}$$

During the sol–gel synthesis of metal doped TiO_2, high water ratio was kept to enhance the nucleophilic attack of water on titanium(IV) isopropoxide and to suppress fast condensation of titanium(IV) isopropoxide species to yield TiO_2 nanocrystals. In addition, the presence of residual alkoxy groups can significantly reduce the rate of crystallization of TiO_2 which favored the formation of less dense anatase phase exclusively [27]. Furthermore, among the two main kinds of crystalline TiO_2, anatase has been confirmed to possess high photocatalytic activity in the photodegradation of most pollutants in water and air, while the photocatalytic activity of rutile is still indistinct. Many reports have shown that the rutile form of TiO_2 is a poor photocatalyst [28–30]. The reasons for this could be attributed that the adsorp-

tive affinity of anatase for organic compounds is higher than that of rutile, and anatase phase also exhibits low rate of recombination in comparison to rutile due to its 10-fold greater rate of hole trapping [31]. The preparation of nano and Zr^{4+} doped TiO_2 were carried out in the presence of acetic acid. Since the pK_a of acetic acid is close to three, there is every chance for protonation of TiO_2 nanoparticles which could suppress further crystallization. In addition, the excess acetate anion adsorbed on the surface of TiO_2 could also suppress the growth of TiO_2. This type of complexation of acetate anion on the surface of anatase form of TiO_2 might be responsible for the decrease in the crystallite size of TiO_2 during the sol–gel synthesis. The addition of acetic acid does not cause residual impurities on the surface of TiO_2 after calcination.

The formation of Ti–O–Zr inhibits the transition of TiO_2 phase and blocks the Ti–O species at the interface with TiO_2 domains stabilizing them, thus preventing the agglomeration of TiO_2 nanoparticles and thus preventing the rutile growth [32]. Hence, the entry of Zr^{4+} in the TiO_2 lattices suppresses the particle growth and consequently increases the band gap values of TiO_2, which minimizes the electron–hole recombination during the photocatalytic degradation of 4-CP. In addition, leaching of metal ions from the TiO_2 lattices during the photocatalytic degradation of 4-CP is not observed. In order to investigate the recyclable efficiency of the catalyst, the suspension after degradation of 4-CP was filtered and washed several times with distilled water and dried at 200 °C. The catalyst was used again for photocatalytic study. There is about 25–30% decrease in TOC removal efficiency of used doped TiO_2 compared to fresh catalyst in the forthcoming three to four cycles. This may be due to blocking of active sites in TiO_2. The XRD patterns of recyclable catalyst show similar patterns compared to fresh catalyst.

4. Conclusions

Zr^{4+} doped TiO_2 nanopowder with high photocatalytic activity can be successfully prepared by sol–gel method. The photocatalytic activity of the doped samples (3 mol% Zr^{4+}) is higher than that of nano TiO_2 and bulk TiO_2 (Dugussa P25). The incorporation of Zr^{4+} in TiO_2 led to small grain size, large surface area and high band gap values. This also led to form more electron capture traps, which contribute to high separation efficiency of photogenerated carriers. The entry of Zr^{4+} into the lattice of TiO_2 is evidenced by XRD, SEM-EDX and fluorescent spectroscopic studies. The photocatalytic degradation of 4-CP over Zr^{4+} doped TiO_2 was revealed higher activity than nano TiO_2 and TiO_2 (Degussa P25). The enhanced adsorption of 4-CP over the catalyst surface and decrease in the particle size as a result of Zr^{4+} doping is suggested to be the cause for high activity of the catalysts. This study therefore suggests that the introduction of metal nitrate can effectively control the selective crystallization of anatase phase of TiO_2. Thus, Zr^{4+} doped TiO_2 photocatalyst system is proven to exhibit high efficiency in the photocatalytic mineralization of 4-CP in aqueous medium.

Acknowledgements

The authors gratefully acknowledge the financial support from the University Grants Commission (UGC), New Delhi, through Centre with Potential for Excellence in Environmental Science in our University. The authors also like to place on record the financial support from the Department of Science and Technology (DST), New Delhi, under FIST programme for the sophisticated equipment facility in the Department. One of the authors, N. Venkatachalam is grateful to the CSIR, New Delhi, India for the award of Senior Research Fellowship.

References

[1] J. Theurich, M. Lindner, D.W. Bahnemann, Langmuir 12 (1996) 6368.
[2] D. Chen, A.K. Ray, Appl. Catal. B: Environ. 23 (1999) 143.
[3] M.A. Fox, M.T. Dulay, Chem. Rev. 93 (1993) 341.
[4] S. Anandan, A. Vinu, N. Venkatachalam, B. Arabindoo, V. Murugesan, J. Mol. Catal. A: Chem. 256 (2006) 312.
[5] M.R. Hoffman, S.T. Martin, W. Choi, D.W. Bahnemann, Chem. Rev. 95 (1995) 69.
[6] G. Rothenberger, J. Moser, M. Gratzel, N. Serpone, D.K. Sharma, J. Am. Chem. Soc. 107 (1985) 8054.
[7] H. Tributsch, in: N. Serpone, E. Pelizetti (Eds.), Photocatalysis: Fundamentals and Applications, Wiley Publishing, New York, 1989, pp. 339–384.
[8] N. Serpone, D. Lawless, J. Disdier, J.M. Hermann, Langmuir 10 (1994) 643.
[9] A. Linsbigler, C. Rusu, J.T. Yates, J. Am. Chem. Soc. 118 (1994) 5284.
[10] A. Di Paola, E.G. Lopez, S. Ikeda, G. Marci, B. Ohatani, L. Palmisano, Catal. Today 75 (2002) 87.
[11] K.E. Karakitsou, X.E. Verykios, J. Phys. Chem. 97 (1993) 1184.
[12] W. Choi, A. Termin, M.R. Hoffman, J. Phys. Chem. 98 (1994) 13669.
[13] N. Serpone, D. Lawless, R. Khairlutdinov, E. Pelizzetti, J. Phys. Chem. 99 (1995) 16655.
[14] G. Cerrato, L. Marchese, C. Morterra, Appl. Surf. Sci. 70 (1993) 200.
[15] A.P. Rivera, K. Tanaka, T. Hisanaga, App. Catal. B: Environ. 3 (1993) 37.
[16] H. Luo, C. Wang, Y. Yan, Chem. Mater. 15 (2003) 3841.
[17] M. Hirano, C. Nakahara, K. Ota, M. Inagaki, J. Am. Ceram. Soc. 85 (2002) 1333.
[18] S. Yuan, P. Meriaudeau, V. Perrichon, Appl. Catal. B: Environ. 3 (1994) 319.
[19] J.C. Yu, J. Yu, W. Ho, L. Zhang, Chem. Commun. (2001) 1942.
[20] Y.M. Wang, S.W. Liu, M.K. Lu, S.F. Wang, F. Gu, X.Z. Gai, X.P. Cui, J. Pan, J. Mol. Catal. A 215 (2004) 137.
[21] S. Sakthivel, M.V. Shankar, M. Palanichamy, B. Arabindoo, D.W. Bahnemann, V. Murugesan, Water Res. 38 (2004) 3001.
[22] K. Nagaveni, M.S. Hegde, G. Madras, J. Phys. Chem. B 108 (2004) 20204.
[23] R.W. Matthews, J. Phys. Chem. 91 (1987) 3328.
[24] B. Neppolian, H.C. Choi, S. Sakthivel, B. Arabindoo, V. Murugesan, J. Hazar. Mater. B 89 (2002) 303.
[25] M.V. Shankar, S. Anandan, N. Venkatachalam, B. Arabindoo, V. Murugesan, Chemosphere 63 (2006) 1014.
[26] X. Fu, L.A. Clark, Q. Yang, M.A. Anderson, Environ. Sci. Technol. 30 (1996) 647.
[27] E.L. Crepaldi, G.J.A.A. Soler-Illia, D. Grosso, F. Cagnol, F. Ribot, J. Sanchez, Am. Chem. Soc. 125 (2003) 9770.
[28] J. Zhu, W. Zheng, B. He, J. Zhang, M. Anpo, J. Mol. Catal. A: Chem. 216 (2004) 35.
[29] J. Zhang, T. Ayusawa, M. Minagawa, K. Kinugawa, H. Yamashita, M. Matsuoka, M. Anpo, J. Catal. 198 (2001) 1.
[30] D.R. Park, J. Zhang, K. Ikeue, H. Yamashita, M. Anpo, J. Catal. 185 (1999) 114.
[31] S. Sakthivel, M.C. Hidalgo, D.W. Bahnemann, S.-U. Geissen, V. Murugesan, A. Vogelpohl, Appl. Catal. B: Environ. 63 (2005) 31.
[32] J. Nair, P. Nair, F. Mizukami, Y. Oosawa, T. Okubo, Mater. Res. Bull. 34 (1999) 1275.